EurJIC
European Journal of Inorganic Chemistry

A Journal of ChemPubSoc Europe

Accepted Article

Title: Easy and green route for nanostructured ZnO as active sensing material with unexpected H2S dosimeter-type behaviour

Authors: Stefano Diodati, Jörg Hennemann, Fernando Fresno, Stefano Gialanella, Paolo Dolcet, Urška Lavrenčič Štangar, Bernd Smarsly, and Silvia Gross

To be cited as: *Eur. J. Inorg. Chem.* 10.1002/ejic.201801334

Link to VoR: http://dx.doi.org/10.1002/ejic.201801334

WILEY-VCH

10.1002/ejic.201801334

WILEY-VCH

FULL PAPER

Easy and green route for nanostructured ZnO as active sensing material with unexpected H_2S dosimeter-type behaviour

Stefano Diodati,[a] Jörg Hennemann,[b,c] Fernando Fresno,[d,e] Stefano Gialanella,[f] Paolo Dolcet,[a,g] Urška Lavrenčič Štangar,[e,h] Bernd M. Smarsly,*[b] and Silvia Gross*[a]

Dedicated to the memory of Prof. Dieter Kohl (Justus-Liebig-Universität Gießen)

[a] Dr. S. Diodati, Dr. P.Dolcet, Prof. Dr. S. Gross
Dipartimento di Scienze Chimiche
Università degli Studi di Padova
Via Marzolo 1, 35131- Padova and INSTM, UdR di Padova, Italy
Email: silvia.gross@unipd.it; sterfano.diodati.it@gmail.com; paolo.dolcet@kit.edu
URL: http://www.chimica.unipd.it/silvia.gross/people.html

[b] Dr. J. Hennemann, Prof. Dr. B. Smarsly
Physikalisch-Chemisches Institut
Justus-Liebig-Universität Gießen
Heinrich-Buff-Ring 17, 35392 Giessen, Germany
Email: bernd.smarsly@phys.chemie.uni-giessen.de
URL: https://www.uni-giessen.de/faculties/f08/departments/physchem/ag-prof-dr-bernd-smarsly

[c] Dr. J. Hennemann
Institut für Angewandte Physik
Justus-Liebig-Universität Gießen
Heinrich-Buff-Ring 16, 35392 Giessen, Germany
Email: Joerg-Hennemann@t-online.de
URL: https://www.uni-giessen.de/faculties/f08/departments/physchem/ag-prof-dr-bernd-smarsly

[d] Dr. F. Fresno
Photoactivated Processes Unit
IMDEA Energy Institute
Avda. Ramón de la Sagra 3, 28935 Móstoles, Madrid, Spain
Email: fernando.fresno@imdea.org
URL: http://www.energy.imdea.org/people/dr-fernando-fresno

[e] Dr. F. Fresno, Prof. Dr. U. Lavrenčič Štangar
Laboratory for Environmental and Life Sciences
University of Nova Gorica
Vipavska 13, 5000 Nova Gorica, Slovenia
Email: Urska.Lavrencic.Stangar@fkkt.uni-lj.si
URL: http://www.ung.si/en/research/laboratory-for-environmental-and-life-sciences/staff/urska-lavrencic-stangar/

[f] Prof. Dr. S. Gialanella
Dipartimento di Ingegneria Industriale
Università degli Studi di Trento
Via Sommarive 9, I-38123, Trento, Italy
Email: stefano.gialanella@ing.unitn.it
URL: https://webapps.unitn.it/du/it/Persona/PER0004889/Curriculum

[g] Dr. P. Dolcet
Institut für Technische Chemie und Polymerchemie (ITCP)
Karlsruhe Institute of Technology (KIT)
Engesserstr. 20 76133 Karlsruhe, Germany

[h] Prof. Dr. U. Lavrenčič Štangar
Faculty of Chemistry and Chemical Technology
University of Ljubljana
Vecna pot 113, 1000 Ljubljana, Slovenia

Supporting information for this article is given via a link at the end of the document

Abstract: Nanostructured ZnO particles were prepared through a straightforward, quick and low-temperature synthesis route involving coprecipitation of the metal precursor salts with oxalic acid, followed by hydrothermal treatment at 135 or 160 °C. The synthesised nanostructured powders were thoroughly characterised by a wide array of analytical techniques from the morphological (Scanning Electron Microscopy –SEM-, Transmission Electron Microscopy -TEM-, Energy-dispersive X-ray Spectroscopy -EDXS-), structural (Powder X-Ray Diffraction -PXRD-, Selected Area Electron Diffraction -SAED-), compositional (X-ray Photoelectron Spectroscopy -XPS-) and physical (thermal stability) point of view. As far as functional applications are concerned, the powders were tested as gas sensor materials for H_2S detection. Thereby these ZnO particles show unexpected gas dosimeter behaviour at 150 °C. Based on these observations and on a comparison with literature a new model for the interaction of ZnO nanostructures with H_2S is proposed.

Introduction

Metal oxides are among the most common and most important binary compounds encountered in materials science and everyday life; among these, zinc oxide enjoys a widespread use in a broad variety of fields (from medicine to optics and electronics).[1-9] ZnO has attracted a great deal of attention due to its semiconductor properties[10-13]. It has a direct wide band gap (3.37 eV) and high exciton binding energy (60 meV):[5-6, 13-16] this property, combined with its availability and relative ease of preparing large and high-quality crystals, though smaller crystals can also display interesting and useful functional properties, makes ZnO a very interesting material for optoelectronics as well as photocatalysis.[17-19]

In other fields, doped and undoped zinc oxide nanowires[19] find diverse applications as biosensors, light emitting diodes and active materials in dye-sensitised solar cells. In addition, ZnO represents a promising material for gas sensors based on semiconducting metal oxides.[20-21] The first investigations were performed in the 1950's, examining the influence of hydrogen (H_2) on the conductance of ZnO. [22] In this process, the adsorbed oxygen on the surface reacts with H_2, and electrons in the material are set free, resulting in a decrease in conductance which can be used as a sensing signal.[23] Since then, many investigations concerning the sensing of different gases like ethanol, carbon monoxide (CO), ammonia (NH_3) or nitrogen dioxide (NO_2) have followed.[24-26] Besides these gases, the detection of hydrogen sulphide (H_2S)[27] is quite an important task, especially in the context of biogas production and use. H_2S is a toxic gas which

leads, for instance, to the corrosion of compressors, gas storage tanks, engines and metallic parts of biogas plants.[28-29] Beyond that, it is also highly harmful to the environment and human health.[30]

Recently, ZnO-based semiconductor gas sensors were introduced,[25, 27] but the underlying physical mechanism seems to be different from the one described above. Huang *et al*. showed that the formation of ZnS on the surface of ZnO nanowires represents an important step in the sensing of H_2S.[31] It is assumed that ZnS protects the surface of ZnO against oxygen absorption whereby the conductance increases. The formation of a ZnS layer on top of ZnO can result in a durable change in conductance.[25] This behaviour makes it possible to design a H_2S gas dosimeter (a type of sensor which detects the total amount of gas by accumulation of gas molecules),[32] where the gas is accumulated either at or in the sensitive layer, consequently causing the change in the sensor signal to depend on the amount of adsorbed gas.[33] Regeneration can be achieved by increasing the temperature,[33] and SEM investigation before gas exposure and after regeneration shows no morphological changes, wherefore ZnO dosimeters seem to be suitable for multiple use (see below).

Documented wet chemistry synthetic protocols for zinc oxides include co-precipitation,[34] miniemulsion synthesis[35] and sol-gel chemistry.[34, 36-40] However, given the significant influence that the particle and crystallite size, as well as the composition (specifically the dopant dispersion and dopant-to-host material ratio), exert on the final properties of the sample, a wet chemistry route is generally preferable, allowing low-temperature crystallisation of the desired product as well as fine control over the reaction pathways.[41-42] Within this framework, hydrothermal synthesis, especially of inorganic binary compounds,[15, 18-19, 42-59] features several advantages over conventional wet-chemistry methods used in the synthesis of inorganic compounds, such as co-precipitation followed by calcination,[60-61] or the Pechini method.[62-65] A further important upside lies within the fact that synthesis takes place at relatively low temperatures.[66-67] By adjusting the treatment temperature and the composition of the reaction medium, the hydrothermal approach furthermore allows to tune the resulting particle size.[66-68] The relatively high autogenous pressures employed during synthesis affect several properties which directly influence solubilisation (such as ionic product, density, viscosity and dielectric constant). These conditions can lead to the solubilisation of normally insoluble precursors under conventional conditions.[41, 69]

In this paper we report an easy, fast, reproducible, green and low-temperature procedure for the hydrothermal synthesis of nanostructured zinc oxide, based on a combination of precipitation of oxalates and hydrothermal treatment, a method already successfully applied to the synthesis of ferrites ($CoFe_2O_4$, $MnFe_2O_4$, $NiFe_2O_4$, and $ZnFe_2O_4$).[70-71] The nucleation and crystallisation mechanism of this oxalate-based hydrothermal synthesis route was recently elucidated for these ferrites by means of in-situ characterisation.[70] In this study, this synthetic protocol was adapted to ZnO due to several important advantages (practical ease, speed, low temperature, aqueous environment *etc*.).[71] Among the advantages of this approach, the fact stands out that all precursors decompose cleanly to non-toxic compounds (in particular both acetylacetonate and oxalic acid decompose to CO_2), sub-200 °C temperatures are employed and the only solvent involved is water, thus satisfying many core principles of the *green chemistry* approach.[71] As far as the zinc precursor is concerned, zinc acetylacetonate was additionally chosen because it is a stable, non-deliquescent compound (unlike for instance $ZnCl_2$) and because it decomposes cleanly in an alkaline environment,[40] albeit non-violently. Zn nitrate was considered less suitable for hydrothermal protocols due to the potentially hazardous decomposition of nitrates yielding NO_x species which may cause a sudden and uncontrolled increase in pressure.

Several synthetic parameters, such as nature and nominal ratio of the employed precursors, the amount of peptising agent and nature of the base employed in the synthesis, as well as treatment temperature and time, were explored in order to optimise the preparation protocol, though only the results of two such syntheses are reported here.

A complete structural and functional characterisation of the samples was conducted using several methods such as X-ray Diffraction (XRD), Scanning Electron Microscopy (SEM), Transmission Electron Microscopy (TEM) and X-Ray Photoelectron Spectroscopy (XPS) (see experimental section below).

In gas-sensing tests, the material showed, besides the “classical” semiconductor gas sensing behaviour at 450 °C, also a gas dosimeter behaviour at an operating temperature of 150 °C. This unexpected behaviour was compared with literature and a new model for the interaction between ZnO gas sensors and H_2S was proposed.

Results and Discussion

Structural investigations

Synthesised samples were firstly characterised from a structural point of view in order to identify the obtained crystalline phases and to evaluate the effect of the different employed synthesis parameters. XRD analyses performed on synthesised ZnO samples (Figure 1) revealed that the compounds were highly crystalline, with only the ZnO hexagonal (wurtzite) phase (PDF 01-079-2205) being visible and no evidence of amorphous or spurious phases. Rietveld refinement performed on the patterns relative to ZnO was only possible through fitting with an anisotropic model, showing that, for all samples, the crystallites display preferential growth along certain vectors. Specifically, the crystallites were larger along the [0002] vector (average of 120 nm) and smaller along the [1011] vector (70 nm), as confirmed by the rod-like shape of the nanostructures (see SEM micrographs below).

10.1002/ejic.201801334

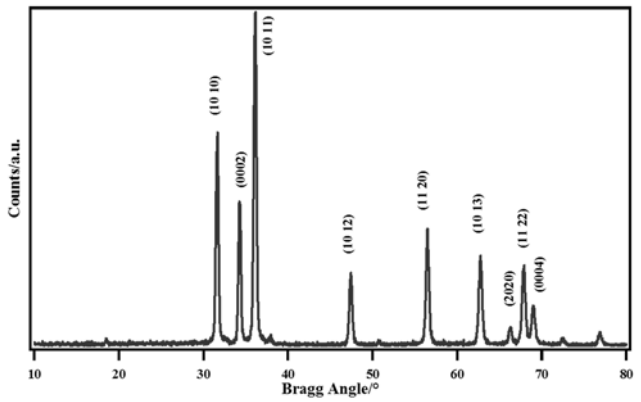

Figure 1. XRD pattern of sample H-ZnO-2with reflections indexed. Given the hexagonal nature of the wurtzite phase, the 4-digit Miller-Bravais notation was preferred to the more common 3-digit Miller hkl notation.

Surface and bulk quantitative analyses

CHN elemental analysis performed on sample H-ZnO-1 (Table 1) showed that minimal organic residues from the synthesis are present in the ZnO sample. This observation can be taken as a further indication of the effectiveness of the synthesis method in preparing compositionally pure materials. In essence, oxalic acid decomposes readily into CO_2 and not into carbonaceous residues, which is a major advantage of this synthetic procedure.

Table 1. Sample composition results (and expected values) from CHN elemental analysis (weight %)

Sample	Content	C [Exp.]	H [Exp.]	N [Exp.]
H-ZnO-1	ZnO	0.07 [0.00]	0.14 [0.00]	0.00 [0.00]

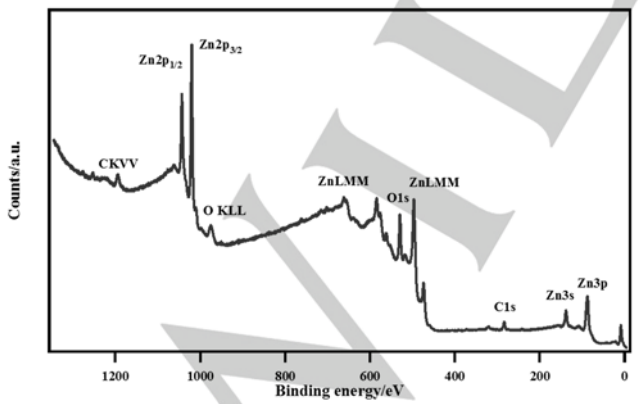

Figure 2. XPS spectrum of ZnO sample H-ZnO-1 (B.E. corrected for surface charging)

Since the ability of a material to function as a sensor or catalyst is highly influenced by its surface chemistry, surface composition of the obtained nanostructured materials was investigated by XPS. Analysis of the XPS spectra for ZnO sample H-ZnO-1 (Figure 2, table 2) shows no sodium or nitrogen, deriving from the precursors, thus confirming that the samples are compositionally pure. Detected binding energies (Table S1 in S.I.) are also in agreement with values found in literature for ZnO.[43, 46, 72-73].

Table 2. Surface concentrations (% at.) for carbon, oxygen, and zinc

Sample	C	O	Zn
H-ZnO-1	16.7	46.0	36.4

Morphology studies

A stable crystalline structure in the sensing material is a necessary feature for reliable gas sensors. Different morphologies of the same sensing material can lead to completely different detected signals.[74] If structural rearrangement occurs during the sensing process, it can impede the gas concentration determination. This problem also notably applies to copper oxide-based H_2S gas dosimeters, which are prepared from nano-granular thin films: they show severe morphological changes during the detection process caused by chemical transformation, which in turn affects the application. As a consequence, in this case, only single-use devices are feasible. However, by obtaining more stable morphologies, reusable gas dosimeters can be developed.[75-76] Within this framework, to gain further insight into the morphology of the synthesised materials, TEM micrographs were acquired (Figure 3). In particular, the bright field image in Figure 3a), shows the elongated, rod-like, shape of the ZnO grains, whose crystallographic structure, in agreement with the XRD data (Fig. 1), is confirmed to be hexagonal (Fig. 3b). The spot pattern in Figure 3c, obtained after tilting along a near axis direction the ZnO grains, indicates that the growing direction of these rod-like structures is [0001].

10.1002/ejic.201801334

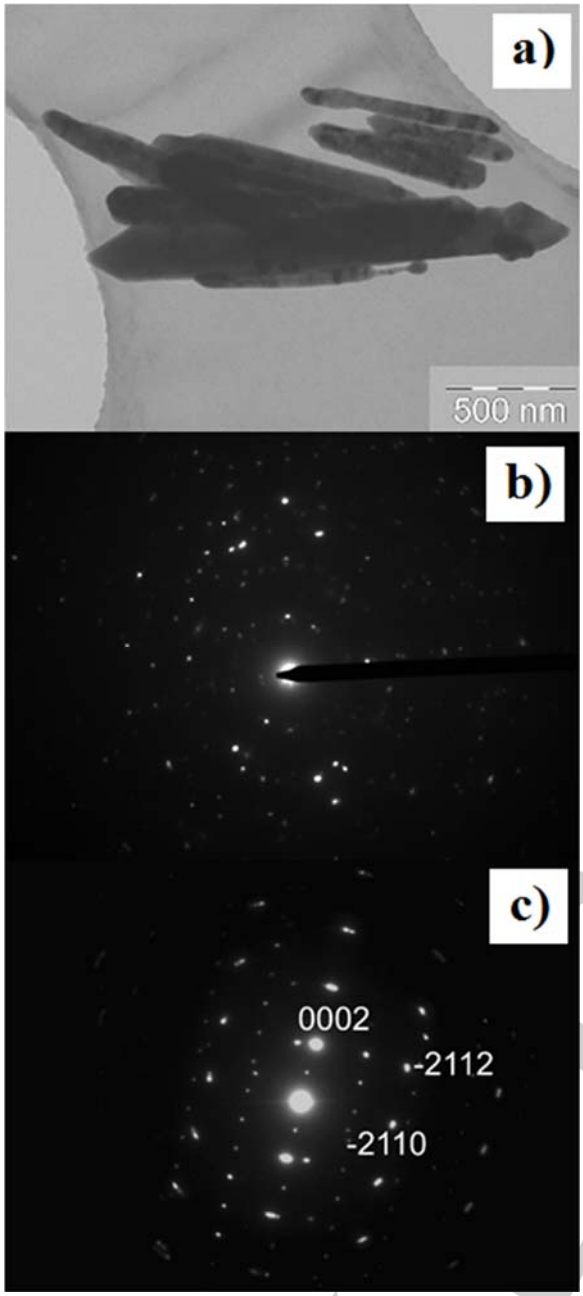

Figure 3. TEM data for sample H-ZnO-1: a) Bright field imaging, showing the rod-like grains; b) SAED patter of the above grains, confirming the hexagonal structure; c) SAED spot pattern in axis direction, indicating the [0001] direction as parallel to the main axis of the grain, parallel to the growth direction

Thermal stability tests

Several practical applications require compounds to operate at high temperatures, particularly gas sensors, where regeneration at several hundred degrees is often necessary in order to maintain a good performance. Within this framework, it was important to investigate structural and morphological stability of the synthesised compounds. Therefore, the materials were heated up to 400 °C (as described in the experimental section), and SEM micrographs were collected before and after (Figure 4) heating. Similarly, XRD analyses were carried out on heat-treated powders (Figure 5).

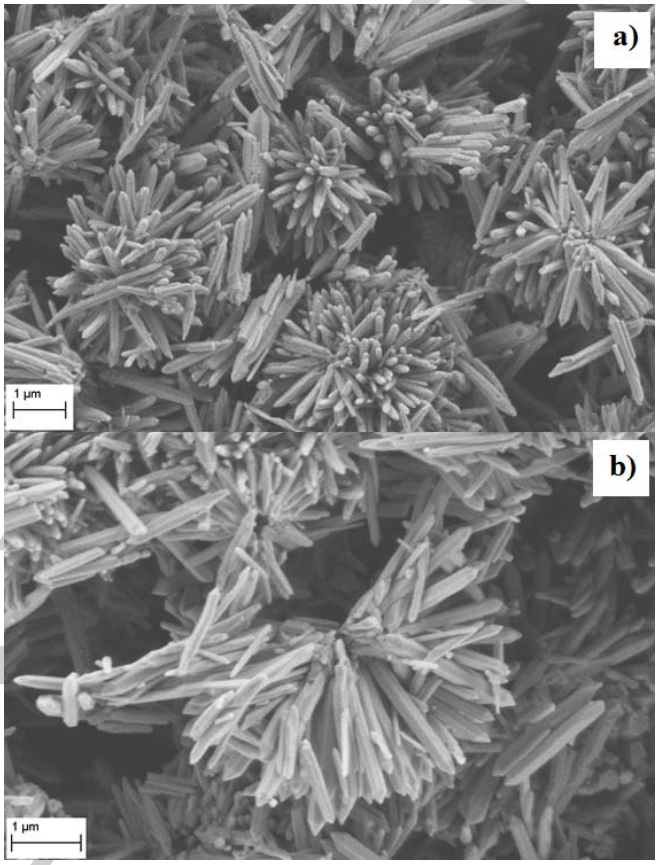

Figure 4. SEM micrograph of ZnO sample H-ZnO-1 before (top) and after treatment at 400°C for 6 h (bottom)

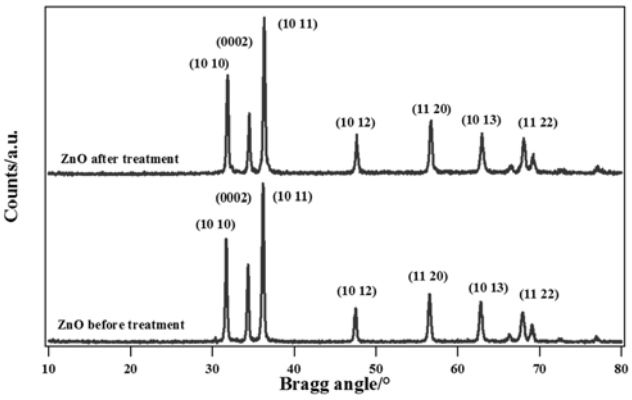

Figure 5. XRD patterns of undoped ZnO before and after thermal treatment at 400°C for 6 h, as indicated.

It is evident from both the micrographs and the XRD patterns that the compound is not subject to any particular degeneration and/or

10.1002/ejic.201801334

morphological change between room temperature and 400 °C, proving that a ZnO material with thermal stability was obtained, in agreement with various literature reports on thermal stability of ZnO[77-79] in air. Calculation of crystallite size through Rietveld refinement also evidenced no notable changes: crystallite sizes remained around 70 nm both before and after treatment. As reported above, and confirmed by SEM analyses, the ZnO nanostructures displayed a strong anisotropy, with the crystallites being larger along the (0002) vector (average of 120 nm) and smaller along the (1011) vector (70 nm). The SEM micrographs provided further confirmation on the ZnO crystalline nanostructures, since the urchin-like morphology evidenced through microscopy (Figure 4) perfectly fits the information reported for ZnO particle growth in basic hydrothermal conditions.[15, 80] It can be argued that the rod-like prismatic grains visible in the TEM micrographs (Figure 3) result from the disruption of the urchin-like structures during ultra-sonication used for sample preparation.

Gas sensing studies

The ZnO sample H-ZnO-1 was also investigated regarding its gas sensing properties. In literature, numerous investigations concerning ZnO applied to the detection of H_2S gas have already been reported.[31, 81-82] In these works, different reactions were observed and relevant mechanisms were proposed, which depend on the gas concentration, operating temperature and size of the ZnO structures. In this context, one must distinguish between surface reactions of H_2S with adsorbed oxygen

$$3\ O_{2\,(ads)}^{-} + 2\ H_2S_{(g)} \rightleftharpoons 2\ SO_{2(g)} + 2\ H_2O_{(g)} + 3\ e^{-} \quad (1)$$

and bulk reactions.

$$ZnO_{(s)} + H_2S_{(g)} \rightleftharpoons ZnS_{(s)} + H_2O_{(g)} \quad (2)$$

Additionally, the following reverse reaction between ZnS and ZnO also plays an important role.

$$ZnS_{(s)} + 3/2\ O_{2(g)} \rightleftharpoons SO_{2(g)} + ZnO_{(s)} \quad (3)$$

To examine the performance of our material, the powder was applied to a commercial gas sensor substrate, as described in the experimental section. After the preparation step, the first gas measurement started at a temperature of 450 °C (Figure 6).

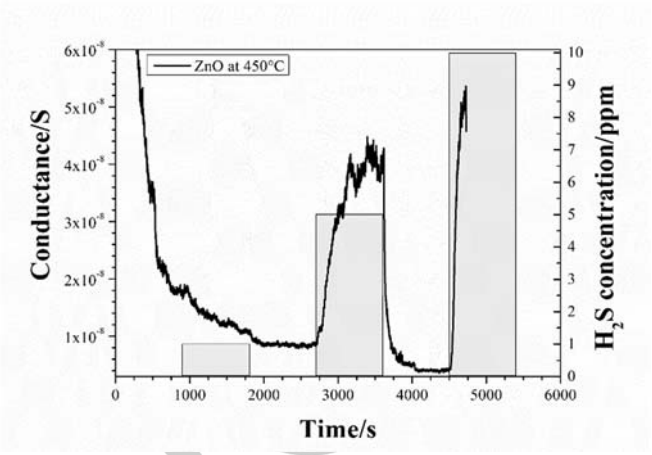

Figure 6. Conductance of the prepared ZnO sensor (powder no. H-ZnO-1) in dependence of different H_2S gas concentrations, measured at an operating temperature of 450° C. After running-in, the sensor shows a typical behaviour of an n-type semiconductor gas sensor.

The sample shows a behaviour typical of a semiconductor-type gas sensor: at the beginning of the measurement, during warm up, the conductance decreases in accordance with the typical behaviour of semiconductors. Upon initial exposure to a low concentration (only 1 ppm) of H_2S, this decrease in conductance is superimposed with and increase caused by the reaction of ZnO with H_2S, in accordance with equation (1). Afterwards, i.e. when removing exposure to H_2S, the conductance signal decreases and stabilises to a constant level (approximately 10^{-8} S). When the second gas exposure (5 ppm H_2S) starts, the conductance increases markedly and converges to a constant value. Removing the H_2S atmosphere, the conductance again decreases substantially before rising steeply upon the third exposure (10 ppm H_2S), substantially exceeding the value obtained for 5 ppm. In essence, Figure 6 shows all the features of the typical behaviour of a semiconductor upon exposure to a reducing gas, i.e. the warm up period, the reaction with H_2S as well as the regeneration between the gas uptakes.

While these measurements were performed at a temperature of 450 °C, during a second set of experiments the sensor was only heated up to 150 °C. Using the same three H_2S concentrations at two significantly different temperatures was intended to provide insight into the underlying chemical process, i.e., if the formation of ZnS from ZnO actually takes place. Indeed, applying a temperature of 150 °C results in a different sensing behaviour (Figure 7).

10.1002/ejic.201801334

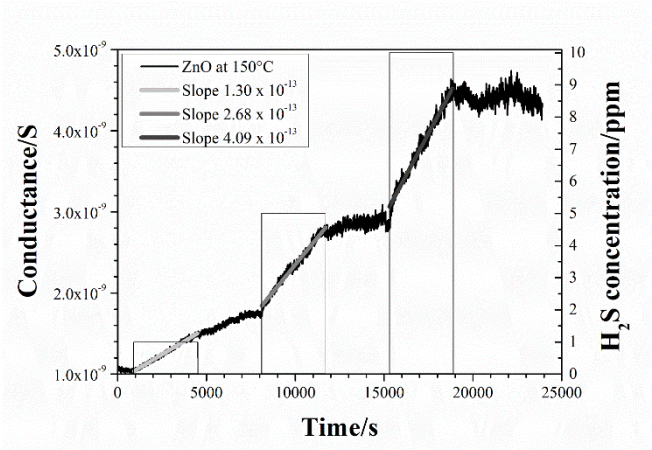

Figure 7. Gas measurement of the same ZnO sensor as in Figure 6 (above) (powder no. H-ZnO-1) applying different H_2S gas concentrations at an operating temperature of 150 °C. The sensor shows a dosimeter-type behaviour.

During these measurements, the conductance levels remain stable during the warm up and prior to the first H_2S exposure. Upon exposure to 1 ppm H_2S the conductance continuously increases following an almost linear behaviour. At the end of the first exposure, the conductance continues to increase, but with a lower slope. The onset of the exposure to 5 ppm H_2S leads to a marked increase in the conductance, with a greater slope as compared to the 1 ppm exposure. Thereafter, the conductance levels off to a constant level. During the exposure to 10 ppm H_2S, the conductance once again increases almost linearly, exhibiting an even sharper slope, remaining nearly constant after interrupting the H_2S exposure. This behaviour is typical of a gas dosimeter[33, 83] and cannot be attributed to surface reactions alone. It is noteworthy to mention that CuO, which is also used as sensor material for the detection of H_2S, shows a similar behaviour at 150 °C. Another interesting and important characteristic of the material can be seen in SEM images: Figure 8 a) shows another sensor, prepared in the same way, before the gas measurement began. In Figure 8 b) the same sensor is shown after sensing measurements performed at 450 °C and regeneration in ambient air for 30 min at 450 °C. A comparison between the corresponding SEM images evidences no apparent alterations to sample structure and morphology. This is a completely different observation in contrast to CuO thin film dosimeters for H_2S, where the structure is substantially altered by the measurement activity (vide supra). In this context, stable structures, which are necessary for a reusable sensor, have so far only been observed with CuO fibres or might be possible with composites.[75, 84-85] The surface composition of the ZnO employed in the dosimeters was also investigated before and after sensing through XPS measurements. XPS analyses carried out on the ZnO sample after use as H_2S dosimeter (prior to regeneration at 450°C) revealed no relevant changes in the binding energies of the Zn2p region (1021.4 eV for $Zn2p_{3/2}$). This was expected since a comparison between ZnO and a ZnS reference revealed very similar Zn2p B.E. values (1021.3-1021.5 eV for $Zn2p_{3/2}$– see Table S1 in S.I.). Quantitative analysis of the XPS spectra however revealed more interesting data: the sample used in H_2S gas sensing experiments displayed a very low sulphur content (1.7% atomic– see Table S2 in S.I.).

Whilst the surface oxygen abundance is a poor indicator of the surface ZnO/ZnS ratio (as surface oxygen may be at least in part due to other species such as carbonates or hydroxides), a comparison between zinc and sulphur atomic percentages reveals that at best only 5.3% of total surface zinc exists as ZnS, with the remaining 94.7% representing oxidised species.

These results, particularly those concerning surface atomic abundance indicate that conversion from ZnO to ZnS during H_2S sensing only occurs at a very thin surface layer. This is consistent with the proposed reaction model (see below).

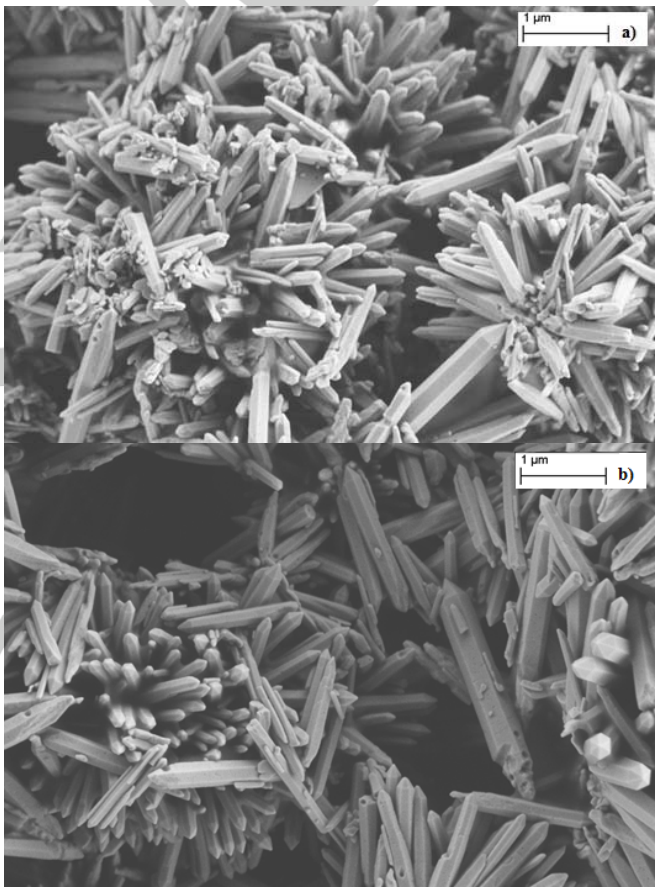

Figure 8. SEM micrographs of the ZnO on a gas sensor substrate a) before gas measurements; b) after gas measurements and regeneration at 450 °C, showing no significant changes and thereby a complete reversibility of the reactions.

In comparison to literature, different models have to be combined to explain the observed conductance behaviour of the ZnO-based material. In the following, the results of these previous studies are presented and discussed in comparison to the results of this work. Thereafter a new model based on all observations will be discussed.

Huang *et al*. examined two types of ZnO materials. First, ZnO nanowire arrays with a thickness of about 50 - 60 nm were investigated at a temperature of 150 °C and exposed to different H_2S concentrations. Second, ZnO microparticles with a structure size of about 150 - 800 nm were exposed to 2000 ppm H_2S in nitrogen at 150 °C.[31] Based on these studies two models including surface and bulk reactions are discussed in the following. The study on nanowires suggests H_2S reacts with ZnO, as described in the above reported equation (2), building up a ZnS layer on the surface of the ZnO grains, as verified by XRD and XPS. This layer protects the interior of ZnO against adsorbing oxygen and avoids binding of electrons. The resulting change in resistance is used as sensor signal. In this instance, the signal is proportional to the gas concentration. When the H_2S flow is turned off, the sensor regenerates in ambient air, according to the chemical reaction (3) and the resistance increases again to its original value. By contrast, the ZnO microparticles do not show such behaviour: only surface reactions take place, as described by equation (1). Due to the greater particle size it was presumed that no sulfurisation takes place at this temperature. This assumption is also supported by the results of Neveux *et al*. showing that smaller ZnO structures have a higher sulfurisation rate compared to larger ones. Similar results are reported by Kim and Yong.[82, 86] However, no dosimeter-type behaviour was observed. Kim and Yong investigated 100-200 nm ZnO structures at temperatures between 300 and 50 0°C under a 50 ppm H_2S gas exposure.[82] They showed via XPS analysis that the sulfurisation process is even more important at higher temperatures. At 200 °C and below, no sulfurisation was observed, in contrast to the results of Huang *et al*.,[31] who on the other hand used nanowires with a thinner diameter. In the model proposed by Kim and Yong, H_2S reacts with the adsorbed oxygen on the surface according to reaction (1). Then electrons are freed and the depletion layer decreases accompanied by an increase in the conductance, which is typical of an n-type semiconductor gas sensor. However, at 300 °C and above, a bulk reaction also takes place as described in equation (2). The formed ZnS should behave like a shallow donor and at the same time a diffusion process should start. Nevertheless, no dosimeter-type behaviour was observed on this occasion too.

Wang *et al*. observed both, a typical semiconducting gas sensor and a dosimeter-type behaviour in ZnO structures measuring about 100 - 400 nm.[81] At temperatures between 350 and 450 °C their measurements show the typical sensor behaviour. The response of the sensor increases directly at the beginning of the gas exposure and slows down when the exposure ends. However, the colder the operating temperature, the slower the regeneration of the sensor. At 150 °C, after an exposure to 20 ppm H_2S, the signal changed only marginally and a regeneration step at 450 °C was added to bring the signal back to its initial value before the gas measurement was started. Only at concentrations considerably below 20 ppm did the sensor signal regenerate at 150 °C. Wang *et al*. posit that the formation of ZnS is responsible for the change of the sensor signal. However, it can also be an indicator of dosimeter behaviour.

The observations and results of these papers, as well as the results of our measurements are summarised in table 3.

Table 3. Summary of the results from the gas measurements obtained in the present study and from the literature

Temp. (°C)	Width (nm)	ZnS	Regen.	Sensor behaviour	Dosimeter behaviour	Ref
150	50-60	Observed by: XRD, XPS	Yes	yes	No	Huang *et al*.[31]
150	100-400	Assumed	Slow at 150° C/ fast at 450 °C	No	Yes	Wang *et al*.[81]
150	150-400	Assumed	At 450 °C	No	Yes	This paper
150	150-800	No	No	No	No	Huang *et al*.[31]
300-500	100-200	Observed by: XPS	Yes	Yes	No	Kim *et al*.[82]
350-450	100-400	No	Yes	Yes	No	Wang *et al*.[81]
450	150-400	Assumed	Yes	Yes	No	This paper

These results show that the behaviour of the ZnO structures strongly depends on both operating temperature and particle size and morphology. Based on previous studies and our own results, the following conclusions can be drawn:

1. At a low operating temperatures, the sulfurisation rate seems to decrease with increasing particle size, which is supported by the work of Neveux *et al*. and Huang *et al*.[31, 86] Note that this effect cannot be simply attributed to the thermodynamic equilibrium of reaction (2), as the reaction of ZnO with H_2S forming ZnS and H_2O is quite exothermic.
2. With increasing particle size, the sulfurisation rate seems to increase at higher operating temperatures[82].

Gas concentration and diffusion processes should nevertheless also be taken into consideration.[81, 86]

Based on this data, we developed a new model for the reaction between H_2S and ZnO, accounting for the sensing behaviour. A schematic overview is given in Figure 9. The model takes into account the interaction of surface reactions, bulk reactions, diffusion processes, operating temperature and particle size.

10.1002/ejic.201801334

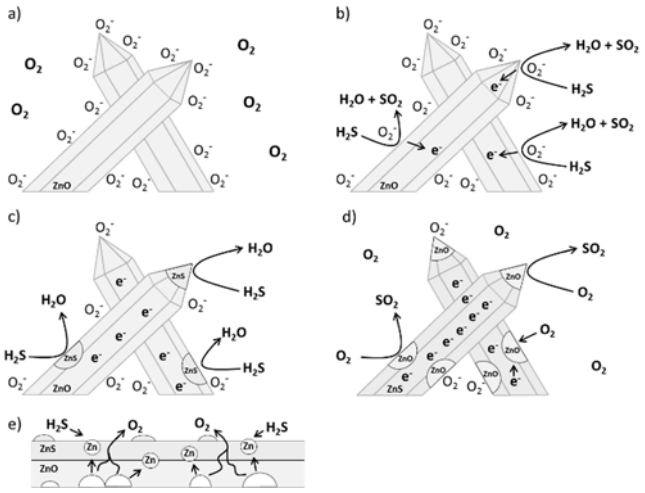

Figure 9. Schematic model for the interaction of ZnO with H_2S at different reaction stages: a) before gas measurements in air; b) surface reactions at the beginning of the H_2S exposure; c) bulk reactions; d) recovery and e) diffusion processes.

Figure 9 a) shows ZnO in air in the absence of any test gases. Oxygen adsorbs at the surface of the n-type semiconducting ZnO, whereby surface acceptor states (binding electrons from bulk) are created. A depletion layer is thus formed in the near-surface area. The depletion layer between two particles hinders the electrons from passing and, as a consequence, the conductance decreases.[23] This model is applicable to both measurements and all regarded systems of Huang *et al*., Wang *et al*., and Kim and Yong as well as particle sizes and temperatures.[31, 81-82]

In Figure 9 b) H_2S gas exposure is initiated. The gas reacts with the adsorbed oxygen, whereby the trapped electrons are set free and decrease the depletion layer. The resulting increase in conductance is proportional to the gas concentration.[23] The reaction mechanism is described by equation (1). Subsequently H_2S reacts with the oxygen to form SO_2 and H_2O.[82] This reaction is applicable to all considered systems at all considered temperatures and both measurements, but can also be just one part of the whole forthcoming mechanism.

The reactions displayed in Figure 9 c) occur subsequently or in parallel to the surface reactions depicted in Figure 9 b). Based on the model by Huang *et al*. H_2S reacts with bulk ZnO, which results in the formation of a ZnS layer on the top of the structure by the ongoing gas exposure.[31] The interior of ZnO is consequently protected against adsorbing oxygen, whereby the electrons in the material remain free and an increase in conductance is preserved. The reaction mechanism for this situation is described by equation (2). This part of the model appears to apply to smaller structures and can be favoured by an increasing operating temperature.[31, 82, 86] With larger structures the sulfurisation rate drops until it is not recognizable any more at low temperatures.[31, 81]

The dimension of the structures (particle size) in our material is intermediate relative to the material from Wang *et al*. and Kim and Yong.[81-82] This feature might be the reason for the dosimeter-type behaviour we observed at 150 °C (Figure 7).[33] At this temperature, the sulfurisation as well as the desulfurisation process can take place. Both were observed by Huang *et al*. with ZnO material samples possessing smaller sizes than in our investigation.[31] The sulfurisation during H_2S exposure and the desulfurisation when the H_2S gas uptake ends are both observed. However, for structures larger than the ones considered in our investigation, Wang *et al*. assumed a sulfurisation process at this temperature but only a weak desulfurisation process.[81] We therefore propose that the particle size of our ZnO material exhibits an optimal precondition for a sulfurisation under H_2S at 150 °C without a desulfurisation process when the gas exposure ends. However, at a higher temperature of 450 °C it behaves like the other reported systems. It is possible that sulfurisation takes place at this temperature, as described by Huang *et al*., but when the H_2S exposure ends the desulfurisation rate is high enough to regenerate the system, in accordance with the impact of temperature on the equilibrium from a thermodynamic point of view.[31, 82]

In Figure 9 d) the regeneration process is shown: ZnS reacts with oxygen to form ZnO and SO_2 as described in equation (3).[31] This reaction occurs at higher temperatures when the gas exposure ends as well as at low temperatures when smaller particles are involved.[31, 81-82] Since ZnO is once again rendered able to adsorb oxygen, free electrons in the material become trapped and as a consequence the conductance decreases.[82]

In addition, diffusion processes can also take place, as depicted in Figure 9 e). A possible process for this situation is described by Neveux *et al*.[86] When ZnO is coated by a ZnS layer, Zn atoms can diffuse to the surface via zinc vacancies, interstitial positions and/or grain boundaries. The same can occur with the remaining oxygen. At the surface, these species can react with H_2S and also form ZnS. As a consequence, vacancies are formed in the interior of the structure and the original grain morphology is lost. This is a very important mechanism, which takes place in parallel to the sulfurisation process and which might lead to an alteration of the materials' structure, which in turn can influence sensing performance, as is the case for CuO thin films interacting with H_2S.[75, 84] This model is a first step to explain the gas sensing behaviour of ZnO structures with H_2S. However, further investigations are needed as gas concentration as well as the relative humidity will have to be considered.

Conclusions

Nanostructured ZnO was synthesised through a quick, easy, low-temperature and green hydrothermal route. The samples were obtained as nanocrystalline powders with high crystallinity and purity and thoroughly characterised from the structural, compositional and morphological point of view.

A particular ZnO sample (H-ZnO-1) shows an interesting gas sensing behaviour. At an operation temperature of 450 °C the material exhibits a significant response to a H_2S gas exposure as expected for a semiconducting n-type gas sensor. However, at an operating temperature of 150 °C the material shows gas dosimeter-type behaviour. Thereby, the slope of the linear increase of conductance depends directly on the offered gas concentration. This interesting property is attributed to the particle

size (ca. 80 nm in diameter), and our proposed mechanism can explain the dosimeter behaviour in relation to this particular particle size. In contrast to CuO thin film H_2S gas dosimeters there are no visible changes in morphology, which can be taken as a proof of an increased dosimeter longevity.

Experimental Section

Chemicals

Tetraethylammonium hydroxide (20% w/w in water) (TENOH), ammonia (28-30% in water), zinc acetylacetonate hydrate and sodium hydroxide were purchased from Sigma Aldrich (Milan, Italy). Oxalic acid dihydrate (99.8%) was purchased from Carlo Erba (Rodano, Milan, Italy). All reagents were used without further purification.

Synthesis protocol

In detail, for the hydrothermal synthesis of a generic ZnO sample, a suspension of zinc oxalate, prepared from an aqueous mixture of zinc acetylacetonate and oxalic acid, was charged in an autoclave, which was heated at a set temperature for a set time span (see Table 4). The reaction scheme, following the protocol explored by Diodati *et al.*[71] is shown in the Supporting Information (Figure S1 in S.I.).

The resulting suspension was sealed in the PTFE cup and placed in a stainless steel container (4745 General Purpose Acid-Digestion Bomb, Parr Instrument Company), heated at a set temperature (135 °C or 160 °C vide infra) for the desired time and then let to cool down by extracting the autoclaves from the oven and leaving them at room temperature in air. The obtained solid powders were isolated by centrifugation, washed four times with deionised water and dried at 90°C in an open air oven. Two different treatment temperatures were explored (135 °C and 160 °C with yields equal to respectively 79 and 71%). The prepared specimens with relative synthesis parameters are listed in Table 4.

Table 4. Synthesis parameters for the various samples

Sample	Target compound	Zn/Acid (mol/mol)	Base	TENOH (mL)	Treatment temp.	Treatment time
H-ZnO-1	ZnO	1/1	NaOH	0.2	135 °C	24 hours
H-ZnO-2	ZnO	1/1	NaOH	0.2	160 °C	24 hours

Powder XRD

PXRD (Powder X-Ray Diffraction) patterns were collected with a Bruker D8 Advance diffractometer equipped with a Göbel mirror and employing the CuK_α radiation. The angular accuracy was 0.001° and the angular resolution was better than 0.01°. All patterns were recorded in the range 10-80° with a scan step 0.03° (2θ) and a 7 second per step acquisition time. Patterns were analysed through the use of the MAUD[87] program, based on a Rietveld refinement, to evaluate the crystallite size of the powders together with other structural and microstructural parameters on the crystalline phases in the samples.

XPS analysis

Samples were investigated by XPS (X-ray Photoelectron Spectroscopy) measurements with a Φ 5600ci Perkin-Elmer spectrometer, using a standard aluminium (Al K_α) source, with an energy of 1486.6 eV operating at 200 W. The X-ray source employed was located at 54.7° relative to the analyser axis. The working pressure was < $5 \cdot 10^{-8}$ Pa ~10^{-11} torr. The calibration was based on the binding energy (B.E.) of the $Au4f_{7/2}$ line at 83.9 eV with respect to the Fermi level. The standard deviation for the B.E. values was 0.15 eV. The reported B.E. were corrected for the B.E. charging effects, assigning the B.E. value of 284.6 eV to the C1s line of carbon.[72, 88-89] Survey scans were obtained in the 0-1350 eV range (pass energy 58.7 eV, 0.5 eV/step, 25 ms/step). Detailed scans (11.75-29.35 eV pass energy, 0.1 eV/step, 50-150 ms/step) were recorded for relevant regions (O1s, C1s, Zn2p, ZnLMM). The atomic composition, after a Shirley-type background subtraction,[90] was evaluated using sensitivity factors supplied by Perkin-Elmer.[72] Assignment of the peaks was carried out according to literature data.

Gas measurements

For the gas measurements 3 mm by 3 mm standard gas sensor substrates from UST GmbH (Geschwenda/Germany) were used. These substrates contain a 10 Ohm built-in platinum heater and platinum inter digital structure (IDS) on top with a gap of ca. 25 µm. The electrical read-out and the heater control were carried out by a homemade electronic setup which is driven by a Lab-View program. Conductance measurements were carried out by applying a constant voltage of 1 V on the IDS.

For the sensor preparation, a 5% w/w suspension of the powder in distilled water was prepared. After stirring, 3µL were deposited onto the IDS of a sensor substrate. Subsequently the substrates were heated up to 400 °C in 30 minutes. This temperature was held for 6 h to calcinate the sensitive layer. The test gas was prepared by a homemade gas mixing device using 500 sccm and 20 sccm mass flow controllers from MKS. For all measurements a gas flow of 200 sccm synthetic air with about 30% relative humidity was used. After an initial time interval to allow for sensor warm-up, a controlled amount of H_2S was added to the gas stream.

CHN elemental analysis (microanalysis)

Samples were introduced in a quartz tube which was kept at 1020 °C and through which a constant flow of oxygen-enriched helium was maintained. The gases resulting from combustion through layers of WO_3 and metallic copper in the primary column were separated by frontal gas-chromatography through the use of a 2 m Porapak QS chromatographic column kept at 190 °C. The separated gas components were then analyzed with a Frison EA 1108 analyzer.

Thermal stability

Compounds were tested for thermal stability by heating 500 mg of the prepared oxide to 400°C with a 200°C/hour ramp. The compounds were kept at 400°C for 3 hours and then left to cool down to RT overnight.

Electron Microscopy (SEM, TEM)

SEM (Scanning electron microscopy) measurements were performed using a Field Emission (FE-SEM) Zeiss SUPRA 40VP, with a primary

beam acceleration voltage of 3 kV and a conventional secondary electron detector for the SEM investigations.

Powder samples were prepared for TEM (Transmission Electron Microscopy) observations. A small amount of each sample was suspended in ethanol using an ultrasonic bath to get rid of agglomeration. A drop of this suspension was deposited onto a holey carbon coated copper grid.

Images of the microstructure and the relevant selected area electron diffraction (SAED) patterns were acquired using an analytical electron microscope (Philips CM12), operated at 120 keV. For the phase identification and indexing of the SAED patterns the Process Diffraction (freeware) software was employed.[91-94]

The SEM images of the gas sensors were taken on a Zeiss Merlin system at an accelerating voltage of 2 kV and a working distance of 2.5 mm.

Acknowledgements

Financial support was provided by the DFG via the GrK (Research training group) 2204 "Substitute Materials for sustainable Energy Technologies". S.G. gratefully acknowledges DFG and the Justus-Liebig Universität Gießen for the provision of a Mercator Fellowship (2016-2020). We would like to thank the Centre of Materials Research (LaMa) at Justus-Liebig Universität Gießen for the support of this project. Furthermore, we would like to thank the DFG for the financial support of our research (KO 719/13-1).

Keywords: hydrothermal synthesis; zinc oxide; gas sensors; dosimeters; functional materials

[1] H. Mirzaei, M. Darroudi, *Ceram. Int.* **2017**, *43*, 907-914.
[2] H. Morkoç, Ü. Özgür, *Zinc Oxide: Fundamentals, Materials and Device Technology, Vol. Weinheim*, Wiley VCH, **2009**.
[3] T. Kim, T. Hyeon, *Nanotechnology* **2014**, *25*, 012001.
[4] S. Chandra, K. C. Barick, D. Bahadur, *Adv. Drug Deliv. Rev.* **2011**, *63*, 1267-1281.
[5] Ü. Özgür, Y. I. Alivov, C. Liu, A. Teke, M. A. Reshchikov, S. Doğan, V. Avrutin, S.-J. Cho, H. Morkoç, *J. Appl. Phys.* **2005**, *98*, 041301.
[6] Z. L. Wang, *J. Phys.: Condens. Matter* **2004**, *16*, R829-R858.
[7] A. B. Djurisic, Y. H. Leung, *Small* **2006**, *2*, 944-961.
[8] J. Gomez, O. Tigli, *J. Mater. Sci.* **2013**, *48*, 612-624.
[9] J. Xu, Z. Chen, J. A. Zapien, C.-S. Lee, W. Zhang, *Adv. Mater.* **2014**, *26*, 5337-5367.
[10] S. J. Pearton, C. R. Abernathy, M. E. Overberg, G. T. Thaler, D. P. Norton, N. Theodoropoulou, A. F. Hebard, Y. D. Park, F. Ren, J. Kim, L. A. Boatner, *Journal of Applied Physics* **2003**, *93*, 1-13.
[11] P. H. Miller, *Phys. Rev.* **1941**, *60*, 890-895.
[12] J. Anderson, G. V. d. W. Chris, *Rep. Prog. Phys.* **2009**, *72*, 126501.
[13] Y. Hou, Z. Mei, X. Du, *J. Phys. D Appl. Phys.* **2014**, *47*, 283001.
[14] R. Suryanarayanan, in *ZnO Nanocrystals and Allied Materials, Vol. 180* (Eds.: M. S. R. Rao, T. Okada), Springer India, **2014**, pp. 289-307.
[15] Y. Xiao, Z. Pan, X. Tian, H. Zhang, X. Zeng, C. Xiao, G. Hu, Z. Wei, *Mater. Lett.* **2014**, *131*, 94-96.
[16] D. Panda, T.-Y. Tseng, *J. Mater. Sci.* **2013**, *48*, 6849-6877.
[17] M. Inoue, N. Hasegawa, R. Uehara, N. Gokon, H. Kaneko, Y. Tamaura, *Sol. Energy* **2004**, *76*, 309-315.
[18] S. K. Kansal, A. H. Ali, S. Kapoor, D. W. Bahnemann, *Sep. Purif. Technol.* **2011**, *80*, 125-130.
[19] Y. Y. Zhang, M. K. Ram, E. K. Stefanakos, D. Y. Goswami, *J. Nanomater.* **2012**, *2012*, 22.
[20] R. Kumar, O. Al-Dossary, G. Kumar, A. Umar, *Nano-Micro Lett.* **2015**, *7*, 97-120.
[21] S. Leonardi, *Chemosensors* **2017**, *5*, 17.
[22] G. Heiland, *Z. Phys.* **1957**, *148*, 28-33.
[23] G. Heiland, *Sensor. Actuator.* **1981**, *2*, 343-361.
[24] A. R. Raju, C. N. R. Rao, *Sensor. Actuat. B-Chem.* **1991**, *3*, 305-310.
[25] J. X. Wang, X. W. Sun, Y. Yang, H. Huang, Y. C. Lee, O. K. Yan, L. Vayssieres, *Nanotechnology* **2006**, *17*, 4995.
[26] M. W. Ahn, K. S. Park, J. H. Heo, D. W. Kim, K. J. Choi, J. G. Park, *Sensor. Actuat. B - Chem.* **2009**, *138*, 168-173.
[27] S. K. Pandey, K.-H. Kim, K.-T. Tang, *TRAC - Trend. Anal. Chem.* **2012**, *32*, 87-99.
[28] A. Wellinger, A. Lindberg, *Biogas upgrading and utilization. Task 24: energy from biological conversion of organic waste*, IEA Bioenergy, **1999**.
[29] D. Schieder, P. Quicker, R. Schneider, H. Winter, S. Prechtl, M. Faulstich, *Water Sci. Technol.* **2003**, *48*, 209-212.
[30] S. Pipatmanomai, S. Kaewluan, T. Vitidsant, *Appl. Energ.* **2009**, *86*, 669-674.
[31] H. Huang, P. Xu, D. Zheng, C. Chen, X. Li, *J. Mater. Chem. A* **2015**, *3*, 6330-6339.
[32] I. Marr, K. Neumann, M. Thelakkat, R. Moos, *Appl. Phys. Lett.* **2014**, *105*, 133301.
[33] I. Marr, A. Groß, R. Moos, *J. Sens. Sens. Syst.* **2014**, *3*, 29-46.
[34] C. Klingshirn, *Phys. Status Solidi B* **2007**, *244*, 3027-3073.
[35] P. Dolcet, F. Latini, M. Casarin, A. Speghini, E. Tondello, C. Foss, S. Diodati, L. Verin, A. Motta, S. Gross, *Eur. J. Inorg. Chem.* **2013**, *2013*, 2291-2300.
[36] L. Spanhel, *J. Sol-Gel Sci. Technol.* **2006**, *39*, 7-24.
[37] L. Spanhel, M. A. Anderson, *J. Am. Chem. Soc.* **1991**, *113*, 2826-2833.
[38] Z. Chen, G. Zhan, Y. Wu, X. He, Z. Lu, *J. Alloy Compd.* **2014**, *587*, 692-697.
[39] E. J. Donahue, A. Roxburgh, M. Yurchenko, *Mater. Res. Bull.* **1998**, *33*, 323-329.
[40] A. Famengo, S. Anantharaman, G. Ischia, V. Causin, M. M. Natile, C. Maccato, E. Tondello, H. Bertagnolli, S. Gross, *Eur. J. Inorg. Chem.* **2009**, *2009*, 5017-5028.
[41] D. R. Modeshia, R. I. Walton, *Chem. Soc. Rev.* **2010**, *39*, 4303-4325.
[42] S. Diodati, P. Dolcet, M. Casarin, S. Gross, *Chem. Rev.* **2015**, *115*, 11449-11502.
[43] O. Lupan, L. Chow, L. K. Ono, B. R. Cuenya, G. Chai, H. Khallaf, S. Park, A. Schulte, *J. Phys. Chem. C* **2010**, *114*, 12401-12408.
[44] W. E. Mahmoud, *J. Cryst. Growth* **2010**, *312*, 3075-3079.
[45] A. Yu, J. Qian, H. Pan, Y. Cui, M. Xu, L. Tu, Q. Chai, X. Zhou, *Sensor. Actuat. B-Chem.* **2011**, *158*, 9-16.
[46] Y. Lu, Y. Lin, D. Wang, L. Wang, T. Xie, T. Jiang, *Nano Res.* **2011**, *4*, 1144-1152.
[47] P. K. Sharma, M. Kumar, A. C. Pandey, *J. Nanopart. Res.* **2011**, *13*, 1629-1637.
[48] C. Wu, L. Shen, H. Yu, Q. Huang, Y. C. Zhang, *Mater. Res. Bull.* **2011**, *46*, 1107-1112.
[49] E. D. Bøjesen, K. M. Ø. Jensen, C. Tyrsted, N. Lock, M. Christensen, B. B. Iversen, *Cryst. Growth Des.* **2014**, *14*, 2803-2810.
[50] X. Zhao, M. Li, X. Lou, *Adv. Powder Technol.* **2014**, *25*, 372-378.
[51] M. Salavati-Niasari, F. Davar, M. Mazaheri, *J. Alloy. Compd.* **2009**, *470*, 502-506.
[52] J.-Y. Park, S.-J. Park, J.-H. Lee, C.-H. Hwang, K.-J. Hwang, S. Jin, D.-Y. Choi, S.-D. Yoon, I.-H. Lee, *Mater. Lett.* **2014**, *121*, 97-100.
[53] S. Li, Z. Wu, W. Li, Y. Liu, R. Zhuo, D. Yan, W. Jun, P. Yan, *CrystEngComm* **2013**, *15*, 1571-1577.
[54] L. M. Gan, B. Liu, C. H. Chew, S. J. Xu, S. J. Chua, G. L. Loy, G. Q. Xu, *Langmuir* **1997**, *13*, 6427-6431.
[55] J. Zhang, S. Liu, J. Yu, M. Jaroniec, *J. Mater. Chem.* **2011**, *21*, 14655-14662.

[56] F. J. Chen, Y. L. Cao, D. Z. Jia, *Chem. Eng. J.* **2013**, *234*, 223-231.
[57] D. Han, J. Cao, S. Yang, J. Yang, B. Wang, L. Fan, Q. Liu, T. Wang, H. Niu, *Dalton Trans.* **2014**, *43*, 11019-11026.
[58] M.-A. Einarsrud, T. Grande, *Chem. Soc. Rev.* **2014**, *43*, 2187-2199.
[59] A. Rabenau, *Angew. Chem. Int. Edit.* **1985**, *24*, 1026-1040.
[60] H. Aono, H. Hirazawa, T. Naohara, T. Maehara, *Appl. Surf. Sci.* **2008**, *254*, 2319-2324.
[61] W. Bayoumi, *J. Mater. Sci.* **2007**, *42*, 8254-8261.
[62] M. Kakihana, M. Yoshimura, *Bull. Chem. Soc. Jpn.* **1999**, *72*, 1427-1443.
[63] P. A. Lessing, *Am. Ceram. Soc. Bull.* **1989**, *68*, 1002-1007.
[64] D. Segal, *J. Mater. Chem.* **1997**, *7*, 1297-1305.
[65] Q.-H. Jiang, C.-W. Nan, Z.-J. Shen, *J. Am. Ceram. Soc.* **2006**, *89*, 2123-2127.
[66] K. Byrappa, M. Yoshimura, *Handbook of Hydrothermal Technology*, Noyes Publications, Park Ridge, New Jersey, U.S.A, **2001**.
[67] L. Dem'yanets, L. Li, T. Uvarova, *J. Mater. Sci.* **2006**, *41*, 1439-1444.
[68] Y. Jin, C. An, K. Tang, L. Huang, G. Shen, *Mater. Lett.* **2003**, *57*, 4267-4270.
[69] U. Schubert, N. Hüsing, *Synthesis of inorganic materials, 2nd Ed.*, Wiley-VCH, Weinheim, **2005**.
[70] P. Dolcet, S. Diodati, F. Zorzi, P. Voepel, C. Seitz, B. M. Smarsly, S. Mascotto, F. Nestola, S. Gross, *Green Chem.* **2018**, *20*, 2257-2268.
[71] S. Diodati, L. Pandolfo, S. Gialanella, A. Caneschi, S. Gross, *Nano Res.* **2014**, *7*, 1027-1042.
[72] J. F. Moulder, W. F. Stickle, P. E. Sobol, K. D. Bomben, *Handbook of X-Ray Photoelectron Spectroscopy - A Reference Book of Standard Spectra for Identification and Interpretation of XPS Data*, Perkin-Elmer Corp., Eden Prarie, Minnesota, **1992**.
[73] *NIST XPS Database - Version 3.5; http://srdata.nist.gov/xps/.*
[74] T. Wagner, C.-D. Kohl, M. Fröba, M. Tiemann, *Sensors* **2006**, *6*, 318-323.
[75] C. Seitz, G. Beck, J. Hennemann, C. Kandzia, K. P. Hering, A. Polity, P. J. Klar, A. Paul, T. Wagner, S. Russ, B. M. Smarsly, *J. Sens. Sens. Syst.* **2017**, *6*, 163-170.
[76] J. Hennemann, C.-D. Kohl, B. M. Smarsly, T. Sauerwald, J.-M. Teissier, S. Russ, T. Wagner, *Phys. Status Solidi A* **2015**, *212*, 1281-1288.
[77] Y. Song, E. S. Kim, A. Kapila, *J. Electron. Mater.* **1995**, *24*, 83-86.
[78] T. Wang, X. Diao, P. Ding, *J. Alloy Compd.* **2011**, *509*, 4910-4915.
[79] D. S. King, R. M. Nix, *J. Catal.* **1996**, *160*, 76-83.
[80] B. Ludi, M. Niederberger, *Dalton Trans.* **2013**, *42*, 12554-12568.
[81] D. Wang, X. Chu, M. Gong, *Nanotechnology* **2007**, *18*, 185601.
[82] J. Kim, K. Yong, *J. Phys. Chem. C* **2011**, *115*, 7218-7224.
[83] A. Geupel, D. Schönauer, U. Röder-Roith, D. J. Kubinski, S. Mulla, T. H. Ballinger, H. Y. Chen, J. H. Visser, R. Moos, *Sensor. Actuat. B - Chem.* **2010**, *145*, 756-761.
[84] J. Hennemann, C.-D. Kohl, B. M. Smarsly, H. Metelmann, M. Rohnke, J. Janek, D. Reppin, B. K. Meyer, S. Russ, T. Wagner, *Sensor. Actuat. B - Chem.* **2015**, *217*, 41-50.
[85] J. Hennemann, T. Sauerwald, C.-D. Kohl, T. Wagner, M. Bognitzki, A. Greiner, *Phys. Status Solidi A* **2012**, *209*, 911-916.
[86] L. Neveux, D. Chiche, D. Bazer-Bachi, L. Favergeon, M. Pijolat, *Chem. Eng. J.* **2012**, *181-182*, 508-515.
[87] L. Lutterotti, Università degli Studi di Trento, Trento, **1998**.
[88] D. Briggs, M. P. Seah, *Practical Surface Analysis - Volume 1 - Auger and X-ray Photoelectron Spectroscopy, 2nd Ed.*, John Wiley & Sons, New York, **1990**.
[89] Z. G. Wang, X. T. Zu, S. Zhu, L. M. Wang, *Phys. E.* **2006**, *35*, 199-202.
[90] D. A. Shirley, *Phys. Rev. B* **1972**, *5*, 4709-4713.
[91] J. L. Lábár, *Ultramicroscopy* **2005**, *103*, 237-249.
[92] J. L. Lábár, *Microsc. Microanal.* **2008**, *14*, 287-295.
[93] J. L. Lábár, *Microsc. Microanal.* **2009**, *15*, 20-29.
[94] J. L. Lábár, M. Adamik, B. P. Barna, Z. Czigány, Z. Fogarassy, Z. E. Horváth, O. Geszti, F. Misják, J. Morgiel, G. Radnóczi, G. Sáfrán, L. Székely, T. Szüts, *Microsc. Microanal.* **2012**, *18*, 406-420.

10.1002/ejic.201801334

WILEY-VCH

Entry for the Table of Contents

FULL PAPER

Nanostructured ZnO was synthesised through a quick, easy, low-temperature and green hydrothermal route, showing an interesting gas sensing behaviour. At an operation temperature of 450 °C the material exhibits a significant response to a H_2S gas exposure as expected for a semiconducting n-type gas sensor. However, at an operating temperature of 150°C the material shows gas dosimeter-type behaviour.

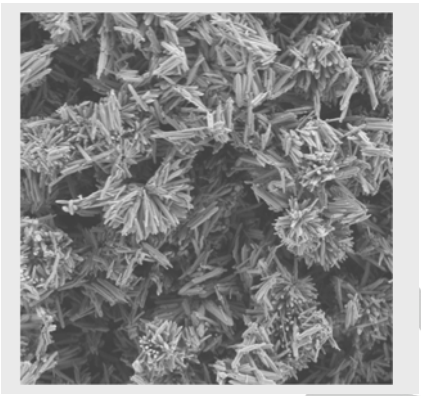

ZnO-based H_2S dosimeters

Stefano Diodati, Jörg Hennemann, Fernando Fresno, Stefano Gialanella, Paolo Dolcet, Urška Lavrenčič Štangar, Bernd M. Smarsly, and Silvia Gross**

Page No. – Page No.

Easy and green route to earth-abundant based functional materials: ZnO as an effective active material for H_2S dosimeters